



1 **Runoff component quantification and future streamflow projection**
2 **in a large mountainous basin based on a multidata-constrained**
3 **cryospheric-hydrological model**

4 Mengjiao Zhang^{1,2}, Yi Nan^{1,2}, Fuqiang Tian^{1,2}

5 ¹Department of Hydraulic Engineering, Tsinghua University, Beijing 100084, China

6 ²National Key Laboratory of Hydrosphere Science and Hydraulic Engineering, Tsinghua University, Beijing 100084,
7 China

8 *Correspondence to:* Yi Nan (ny1209@qq.com); Fuqiang Tian(tianfq@tsinghua.edu.cn)

9 **Abstract.** The Yarlung Tsangpo River (YTR) is one of the several major rivers originating from the Tibetan Plateau (TP)
10 and plays a pivotal role in providing invaluable fresh water to its downstream countries. Large uncertainties existed in the
11 studies related to streamflow variations in this basin, and the investigation is difficult due to the widely distributed
12 snowpack, glaciers and permafrost and their complex effects on hydrological processes. In this study, we conducted a
13 systematic analysis on the streamflow variations and runoff components in the YTR basin, using a physically-based
14 hydrological model validated by streamflow and multiple datasets related to cryospheric processes. Main findings include
15 (1) The contributions of snowmelt and glacier melt runoff to streamflow were limited, both for about 5~6% for the whole
16 basin, which might be overestimated by previous studies. (2) Under the climate change, the annual runoff would increase
17 evidently in the future. The relative change of annual streamflow could exceed 90mm (~38%) at the outlet station in the
18 far future compared to the historical period under the high emission scenario, while the amount and contributions of
19 meltwater runoff would both decrease. (3) Adopting more observational data to calibrate the hydrological model played a
20 critical role in reducing the uncertainty of hydrological simulation. The biases of snow and glacier simulation for data
21 unconstrained led to a marked overestimation of contributions of snowmelt and glacier melt runoff to streamflow and
22 further brought about an underestimation of the increasing trends of annual runoff by approximately 5~10% in future
23 projection. These results provide a relatively reliable reference of the streamflow change and the runoff components in
24 both historical and future periods in the YTR basin, and have the potential to serve as a “reference value” in this region
25 because we used more datasets to constrain the model uncertainty compared to previous studies.
26



27 **1. Introduction**

28 The Tibetan Plateau (TP), widely known as the “Asian Water Tower”, is the source region of many large rivers in Asia
29 and plays a pivotal role in providing invaluable fresh water to its downstream countries. The hydrological changes in the
30 TP region have drawn high attention for a long time and there have been numerous relevant researches on its hydrological
31 process. However, further study is necessary to fully understand the streamflow conditions of the TP and there is still a lot
32 of uncertainty in its runoff variations.

33 On the one hand, the special environmental conditions increase the complexity of hydrological processes in the TP
34 region. Vast areas of snow, glaciers, permafrost and seasonally frozen ground distribute over the TP throughout the year
35 and all cryospheric components can contribute to streamflow in various ways (Lan et al., 2014). Understanding their impact
36 on hydrological processes is crucial for a confident prediction of runoff change under climate warming. Yet, this is a
37 difficult task because the complex hydrological and cryospheric processes were typically insufficiently represented by
38 hydrological models (Nan et al., 2022). On the other hand, marked atmospheric warming has changed the water balance of
39 the TP and altered water resources in downstream countries (Yao et al., 2022). Remarkably, TP is one of the most significant
40 regions responding to climate change and the effects of climate change on water availability differ substantially among
41 basins (Immerzeel et al., 2010). Also, the continuous rising temperature leads to rapid retreat of perennial snow and glaciers,
42 impacting runoff and regional water security as well (Chen et al., 2017).

43 The Yarlung Tsangpo River (YTR), also termed as Brahmaputra after it flows into India, is one of the several major
44 rivers originating from the TP and the largest river system in the south TP. As a representative river basin of the TP, the
45 dynamic interactions between cryosphere, hydrosphere and atmosphere are prominent in the YTR basin, in which the
46 hydrological processes like snow and glacial melting are more vital compared to some other regions, and the hydrological
47 processes are complicated and sensitive to climate changes with high uncertainty (Jiang et al., 2022; Xu et al., 2019). Many
48 studies have been conducted on the analysis of runoff compositions in the YTR basin but the results are not all consistent,
49 while studies to examine the impacts of climate change on the hydrology and water resources of this basin are still limited
50 (Xu et al., 2019).

51 Monitoring of hydrological stations is critical to investigate the changes in streamflow and is the prominent data
52 source for related study. Observational evidence demonstrates substantial increases in both annual runoff and annual
53 sediment fluxes in the headwaters of TP across the past six decades (Li et al., 2021). But further research on the composition
54 and future changes of streamflow still relies on hydrological models for now. Distributed hydrological model is an essential
55 tool for study on the hydrological process of basins while the difficulty is that the model parameters are physically
56 insufficient with large uncertainty, due to the limited observation data to calibrate the model (Tian et al., 2020). There have
57 already been many studies trying to simulate the hydrological processes more realistically, including considering the
58 contributions of snow and glacier (Zhang et al., 2013; Chen et al., 2017), simulating seasonal permafrost (Wang et al.,
59 2023), and developing tracer-aided hydrological models (Nan et al., 2022). Utilizing more datasets to evaluate the model
60 performance is supposed to be a feasible way to constrain modeling uncertainty.

61 In this study, we conducted a systematic analysis on the streamflow change in the YTR basin based on observation
62 streamflow data and various datasets related to cryospheric processes. We focused on the streamflow change during the
63 historical period, the contribution of multiple runoff components, and the trend in the future period. We conducted different
64 calibration variants to evaluate the value of different datasets on the model performance and the consequent impacts on the
65 runoff component partitioning and future projection results. We structured the paper into the following sections. Section 1
66 formulates the background of this study. Section 2 briefly introduces the YBR basin, followed by the used materials and
67 methods. The main results are presented in Section 3. A brief discussion including a comparison with previous studies are



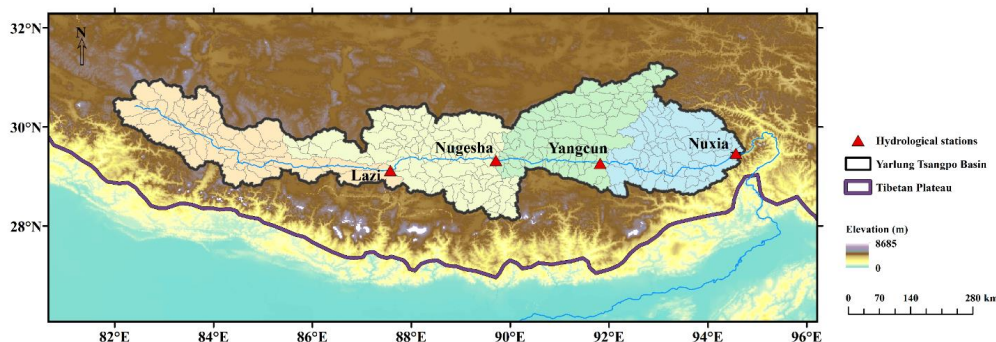
68 in Section 4, followed by the conclusions in Section 5.

69 2. Materials and methodology

70 2.1 The Yarlung Tsangpo River

71 Located on the north of the Himalaya Mountains in the southern TP, the YTR originates from the Gyima Yangzoin
72 glacier at the northern foot of the Himalayas and then travels through China, Bhutan, and India before emptying into the
73 Bay of Bengal in the Indian Ocean. The length of the main stream is over 2000 km and there are four streamflow gauging
74 stations distributed along it, including Lazi, Nugesha, Yangcun, and Nuxia station from upstream to downstream (Tian et
75 al., 2020, red triangle in Fig. 1). The Nuxia station near the border of the TP is selected as the basin outlet of the study area,
76 with a total drainage area of approximately 2×10^5 km² (Fig. 1). The average elevation of the YTR basin is about 4850m
77 a.s.l. (above sea level), with an extent of 1890–6840m.

78 The mean temperature of the basin is relatively low (~ -3.1 °C, 1979–2018) due to the high altitude, while the
79 precipitation is mostly driven by the South Asian monsoon, with an average annual precipitation of about 475mm (1979–
80 2018). Large amounts of moisture from the Indian Ocean entering the plateau water cycle through precipitation can
81 significantly supplement its water resources (Zhou et al., 2019), with an obvious wet season from June to September, which
82 accounts for 60–70% of the total annual rainfall (Xu et al., 2019). Moreover, the changes of the precipitation and runoff
83 demonstrate strong consistency in the exoreic TP rivers, including the YTR (Tian et al., 2023). The average snow cover
84 area is 16.8%, and glaciers cover ~ 2.1 % of the basin (He et al., 2021), resulting in a considerable contribution of meltwater
85 to runoff.



86
87 **Figure 1** Study area and locations of the hydrological stations.

88 2.2 Data

89 2.2.1 Hydrological station data

90 Extensive streamflow measurements were collected at four hydrological stations for variation analysis and
91 hydrological model evaluation. The monthly/annual observations during 1960–2020 were obtained for trend testing, and
92 daily data covering the model simulating period were obtained for model calibration. It should be noted that due to data
93 confidentiality requirements, the measured discharge in the results part were not presented directly by normalization or
94 hiding the vertical coordinates.

95 **Table 1** Basic information of hydrological stations used in the study area.



Station	Longitude (°E)	Latitude (°N)	Altitude (m)	Drainage area (km ²)	Period of observational streamflow	
					Daily	Monthly / Annual
Lazi	87.576	29.121	4003	52516	1980–2020	1960–2020
Nugesha	89.712	29.325	3850	113758	1960–2020	1960–2020
Yangcun	91.822	29.266	3627	164518	1960–2020	1960–2020
Nuxia	94.567	29.467	2955	206019	1960–2020	1960–2020

96

97 2.2.2 Data for model driving and calibration

98 Daily meteorological inputs mainly include precipitation, temperature, and potential evapotranspiration (PET).
 99 Precipitation data of the YTR basin were collected from the 0.1° grid China Meteorological Forcing Dataset (CMFD, Yang
 100 et al., 2019) while temperature and potential evapotranspiration were obtained from the 1.0° grid reanalysis dataset
 101 ERA5_Land for the historical calibration and validation periods. Underlying surface inputs consist of topography, glacier,
 102 vegetation coverages and soil parameters. Elevation was derived from a digital elevation model (DEM) with a spatial
 103 resolution of 30 m from the Geospatial Data Cloud (<https://www.gscloud.cn>). The second glacier inventory data set of
 104 China (Liu, 2012) was used to denote the glacier coverage. Vegetation coverages were extracted from the MODIS satellite
 105 products of 8-day leaf area index (LAI) dataset MOD15A2H (Myneni et al., 2015) and monthly normalized difference
 106 vegetation index (NDVI) dataset MOD13A3 (Didan, 2015). Soil types and properties were collected from Global high-
 107 resolution data set of soil hydraulic and thermal parameters (Dai et al., 2019). For future hydrological simulations, data
 108 from 10 CMIP6 (Coupled Model Intercomparison Project Phase 6, <https://esgfnode.llnl.gov/search/cmip6/>) GCMs
 109 were used as climate inputs, with more detailed introduction in 2.2.3.

110 For the calibration in the historical periods, in addition to the observational daily streamflow during 1980–2018 at the
 111 four stations mentioned in 2.2.1, datasets of snow and glacier were adopted to evaluate the hydrological model. The snow
 112 depth (SD) dataset for TP (Yan et al., 2021)), the Tibetan Plateau Snow Cover Extent product (TPSCE, Chen et al., 2018)
 113 and the Glacier mass balance data (Hugonnet et al., 2021) were used to calibrate SWE (snow water equivalent), SCA (snow
 114 cover area) and GMB (glacier mass balance) respectively. More details of the datasets above can be found in Table 2. Here,
 115 the SD measurements were transferred to SWE for calibration using the following Eq. (1) (Chen et al., 2017):

$$116 \quad SWE = \frac{\rho_{snow} \times SD}{\rho_{water}} = \frac{0.1966 \times SD^{0.9063}}{\rho_{water}} \quad (1)$$

117 where ρ_{snow} is the snow density, SD is the PMV-based snow depth of snowpack, and ρ_{water} is the density of liquid water.
 118 The coefficients were estimated by in situ data.

119 **Table 2** Data from global and regional datasets used for hydrological models in this study.

Datasets as inputs of the hydrological model				
Dataset	Source/Name	Temporal resolution /Period	Description/Notes	Reference and/or Website for download
Precipitation	CMFD (China Meteorological Forcing Dataset)	Daily, 1979–2018	0.1° grid, its accuracy for China is better than that of the internationally available reanalysis data	Yang et al. (2019)
Temperature	ERA5_Land	Daily, 1950–2020	1.0° grid, a reanalysis dataset providing a consistent view of the evolution of land variables over several decades at an enhanced resolution compared to ERA5	https://cds.climate.copernicus.eu/cdsapp#!/dataset/
PET (potential evapotranspiration)				
Topography	SRTM DEM	–	30m spatial resolution	https://www.gscloud.cn/
NDVI (normalized difference vegetation index)	MOD13A2	Monthly, 2000–2020	0.5 arc degree grid, derived from the Advanced Very High Resolution Radiometer (AVHRR) sensors	Didan et al. (2015)



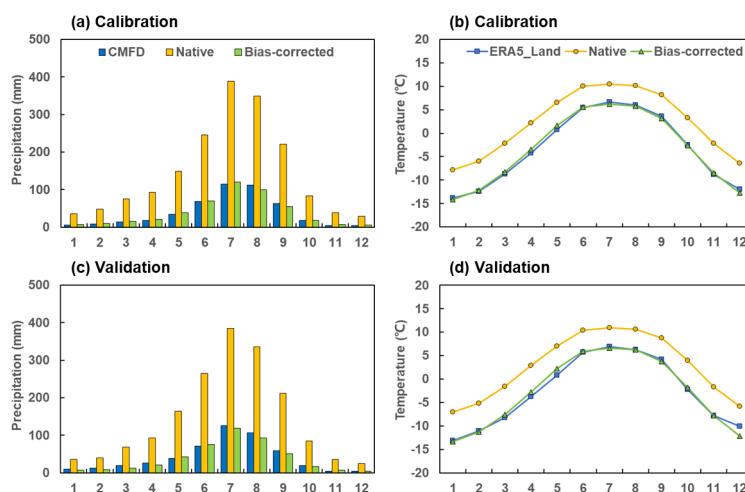
LAI (Leaf Area Index)	MOD15A2H	8-day, 2000–2020	0.05° grid, derived from the Advanced Very High Resolution Radiometer (AVHRR) sensors	Myneni et al. (2015)
Soil	Global high-resolution data set of soil hydraulic and thermal parameters	–	Optimal soil water retention parameters obtained from ensemble pedotransfer functions	Dai et al. (2019), http://globalchange.bnu.edu.cn/research
Glacier distribution	SCGI (The second glacier inventory data set of China)	2006–2011	Clear and concise overview and scientific assessment of the glaciers in China	Liu et al. (2012)
Climate (Precipitation and Temperature)	CMIP6 GCMs	Daily, ~2100	More details in Table 3	https://esgfnode.llnl.gov/search/cmip6/
Datasets for calibration of the hydrological model				
Observational streamflow	Relevant hydrology Bureau	Daily, ~2020	More details in Table 1	–
SD (snow depth)	A daily, 0.05° Snow depth dataset for Tibetan Plateau (2000–2018)	Daily, 2000/9/1–2018/8/31	0.05° grid, based on the snow cover probability in the Tibetan Plateau	Yan et al. (2021)
SCA (snow cover area)	TPSCE (Long-term TP daily 5-km cloud-free snow cover extent record)	Daily, 1981/8/1–2014/12/31	5-km cloud-free snow cover extent record derived from AVHRR surface reflectance CDR	Chen et al. (2018)
GMB (glacier mass balance)	Glacier mass balance data	Annual, 2000–2019	standardized observations on changes in mass, volume, area and length of glaciers over time	Hugonnet et al. (2021)

120

121 2.2.3 Bias-corrected GCMs data

122 The general circulation models (GCMs) are commonly used to simulate the earth’s climate change and project the
 123 future climate change under a suite of different possible emission scenarios. Coupled Model Intercomparison Project Phase
 124 6 (CMIP6) is the latest available CMIP simulations, which is improved comparing to the previous phase. Nevertheless, the
 125 CMIP6 GCMs still have diverse deviations at the regional scale. Taking the TP region for instance, most models
 126 underestimate the observed trends in mean and extreme temperature and precipitation (Cui et al., 2021).

127 Based on the time scale and the simulation performance, ten CMIP6 CGMs data (precipitation and temperature) were
 128 used to conduct this study and their basic information is shown in Table 3. The CMIP6 data during 1960–2100 were
 129 interpolated from various spatial resolutions into the same degree (0.1° grid) through a bilinear interpolation scheme. The
 130 biases in the interpolated data were further corrected against the historical data (CMFD and ERA5_Land, using 1979–2009
 131 as the reference period for correction, and 2010–2018 for validation) based on a multiplicative bias-correction approach
 132 (MBCn algorithm, Alex J. Cannon, 2018; Cui et al., 2023). The average precipitation and temperature of the corrected
 133 GCMs are presented in Fig. 2. When driving the future model, the future PET data was calculated with CMIP6 temperature
 134 data and the historical temperature-PET correlation, and other input data was kept same as the historical period.



135

136

137

Figure 2 Seasonal cycles of precipitation (a) and (c) and temperature (b) and (d) calculated from the historical data (CMFD/ERA5_Land), the ensemble mean of 10 native and bias-corrected CMIP6 data during the calibration (1979–2009) and validation (2010–2018) period.

138

Table 3 Basic information of ten CMIP6 GCMs used in this study.

No.	Name	Nation	Resolution (Lon×Lat)	Period
1	ACCESS-ESM1-5	Australia	1.875°×1.2143°	1950–2100
2	BCC-CSM2-MR	China	1.125°×1.125°	1950–2100
3	CNRM-CM6-1	France	1.40625°×1.40625°	1950–2100
4	GFDL-ESM4	U.S.	1.25°×1°	1950–2100
5	INM-CM5-0	Russia	2°×1.5°	1950–2100
6	MIROC6	Japan	1.40625°×1.40625°	1960–2100
7	MPI-ESM1-2-HR	Germany	0.9375°×0.9375°	1960–2100
8	MPI-ESM1-2-LR	Germany	1.875°×1.875°	1950–2100
9	MRI-ESM2-0	Japan	1.125°×1.125°	1950–2100
10	NESM3	China	1.875°×1.875°	1950–2100

139

2.3 Hydrological model

140

141

142

143

144

145

A spatially-distributed physically-based hydrological model, the Tsinghua Representative Elementary Watershed (THREW) model (Tian et al., 2006) was adopted to simulate streamflow of the YTR basin. This model uses the representative elementary watershed (REW) method for spatial discretization of catchments (Reggiani et al., 1999) and the YTR basin was divided into 276 REWs based on DEM data, as shown in Fig. 1. Areal averages of the gridded estimates of meteorological variables, vegetation cover, soil property, and CMIP6 data were calculated in each REW to drive the model.

146

147

148

149

150

151

For application in cold mountainous regions, the THREW model is incorporated with modules characterizing cryospheric hydrological processes including snowpack dynamics and glacier evolution, and has been successfully applied in several basins across China and the world (Xu et al., 2019; Tian et al., 2020; Nan et al., 2022; Cui et al., 2023). A detailed description of the snow and glacier modules could be found in Cui et al. (2023). Here a modification was made upon the simulation of snowpack accumulation and melting processes on the basis of the model in Cui et al. (2023). The snow sublimation was newly taken into account, similar to Han et al. (2019). In specify, the amount of snowfall entering the



152 runoff-generation process was deducted by a certain proportion of sublimation and two additional parameters were
 153 introduced for this simulation. The details of the calibrated parameters of the THREW model in this study could be found
 154 in Supplementary Table 1.

155 There are two definitions to quantify the contributions of runoff components to streamflow in the THREW model.
 156 One was based on the individual water sources in the total water input triggering runoff processes, including rainfall,
 157 snowmelt, and glacier melt and another was based on pathways of runoff-generation processes, resulting in surface and
 158 subsurface runoff (baseflow) (Nan et al. 2022). Here we focused on the first definition and calculated the contributions of
 159 different water sources (rainfall, snowmelt, and glacier melt) to the total runoff. It should be noted that in the THREW
 160 model, the total discharge was equal to the sum of these three components minus evaporation, thereby achieving the water
 161 balance.

162 2.4 Model calibration

163 Considering the time period of multiple datasets, the simulation period was selected as 1980-2018, and was divided
 164 into two periods by 2009 (i.e. 1980–2009 for calibration and 2010–2018 for validation). Automatic calibration was
 165 implemented by the pySOT (Python Surrogate Optimization Toolbox) algorithm to obtain the multiple-optimal objective
 166 (Eriksson et al. 2019). The Nash-Sutcliffe efficiency coefficient (NSE) and the logarithmic Nash-Sutcliffe efficiency
 167 coefficient (lnNSE) were used together to optimize the simulation of discharge, which can assess the simulations of both
 168 high flow and baseflow processes. The root mean square error (RMSE) was used for the evaluation of SWE, SCA and
 169 GMB simulation. More details about these metrics are presented in Table 4.

170 To assess the effect of various datasets on calibration and their impact on simulation results, in addition to the scenario
 171 taking all the elements (discharge, SWE, SCA, GMB) into consideration, we deleted different elements from the calibration
 172 objectives to form different comparative variants. Thus, there were four variants for comparison: (1) D, calibration solely
 173 using discharge, (2) DG, calibration using discharge and GMB, (3) DS, calibration using discharge, SWE and SCA, (4)
 174 DSG, calibration using discharge, SWE, SCA and GMB. A plainer description of calibration variant designation was as
 175 shown in Table 5. For these variants, the model is calibrated for the whole basin, i.e., the discharge of basin outlet (Nuxia
 176 station) and the basin-scale average values of other elements (SWE, SCA, GMB) were compared between simulations and
 177 observations to evaluate the model. Correspondingly, the value of parameter was assumed to be universal for all the REWs
 178 of the basin.

179 Furthermore, an additional variant was added on the basis of variant “DSG”, referred to as “ALL”. It also considered
 180 all elements, but the discharge data at upstream stations were used for calibration to better consider the spatial heterogeneity
 181 within the basin. In the “ALL” variant, the model used four different sets of parameters for the four sub-regions divided by
 182 four hydrological stations. The adopted parameters of the THREW model in the YTR basin by all calibration variants are
 183 provided in Supplementary Table 2.

184 **Table 4** The calibration elements and the metrics used to evaluate the model performance in this study.

Element	Timescale	Unit	Metrics	Formula	Range	Ideal value
Discharge	Daily	m ³ /s	NSE (Nash Sutcliffe coefficient)	$NSE = 1 - \frac{\sum_{i=1}^n (Q_{o,i} - Q_{s,i})^2}{\sum_{i=1}^n (Q_{o,i} - \bar{Q}_o)^2}$	(-∞, 1)	1
			lnNSE (logarithmic Nash Sutcliffe efficiency coefficient)	$lnNSE = 1 - \frac{\sum_{i=1}^n (\ln Q_{o,i} - \ln Q_{s,i})^2}{\sum_{i=1}^n (\ln Q_{o,i} - \ln \bar{Q}_o)^2}$	(-∞, 1)	1
SWE	Annual	cm	RMSE (Root mean square error)	$RMSE = \sqrt{\frac{\sum_{i=1}^n (A_{o,i} - A_{s,i})^2}{n}}$ ("A" can be replaced by SWE, SCA or GMB)	(0, +∞)	0
SCA		–				
GMB		m/a				



Note: n is the total number of observations, subscripts of "o" and "s" refer to observed and simulated variables, respectively.

185 **Table 5** Five calibration variants of the THREW model in this study.

No.	Objective of calibration	Abbreviation	Notes
1	Discharge	D	Only discharge was considered
2	Discharge + GMB	DG	Snow elements not calculated
3	Discharge + SWE + SCA	DS	Glacier element not calculated
4	Discharge + SWE + SCA + GMB	DSG	All elements were considered (Variant "ALL" used 4 stations, while the others used Nuxia station only)
5		ALL	

186 2.5 Analysis on the streamflow change

187 2.5.1 Historical trend

188 To analyze the trend and change-point of runoff, the Pettitt test and linear regression methods were adopted with the
 189 monthly/annual runoff observations during 1960–2020 at the four hydrological stations (Zhang et al., 2024). Pettitt test is
 190 a non-parametric approach to the change-point problem (Pettitt, 1979), which can be used for mutation analysis of
 191 hydrological sequences to test the abrupt change points. And after obtaining the abrupt change point of the runoff in the
 192 historical period (1960–2020), if the periods divided by it is still long (>20a), the test will be conducted again to obtain
 193 the abrupt change points relative to the primary abrupt change point. Linear regression method is commonly used to analyze
 194 the long-term evolution characteristics of hydrological sequences, reflecting the overall trend and then providing guidance
 195 for water resource utilization. Here the linear regression method was used to calculate the rate of change and the t-test
 196 method was used to determine the significance, quantitatively reflecting the variation trend of runoff over time.

197 2.5.2 Future projection

198 As mentioned in section 2.2.3, 10 CMIP6 GCMs were used in this study and bias correction has been conducted upon
 199 the GCMs based on observation data. Although the bias correction process modified the mean values of precipitation and
 200 temperature, their variation characteristics in the future were mostly preserved, exhibiting significantly rising precipitation
 201 and temperature in the future (Supplementary Fig. 1). Then the observation-constrained THREW model in the YTR basin
 202 was driven by the bias-corrected CMIP6 data under the historical period (1960–2014) and the future period (2015–2100)
 203 under three Shared Socioeconomic Pathways (SSPs) scenarios, i.e., SSP 1-2.6 (SSP126), SSP 2-4.5 (SSP245) and SSP 5-
 204 8.5 (SSP585). The results simulated by models of different calibration variants, and under different future SSP scenarios
 205 were both compared in this study. In the meantime, considering the time period for model calibration and GCMs' bias
 206 correction, the results during 1980–2009 was used as the baseline of historical simulation and two periods (2020–2049 as
 207 Near future, 2070–2099 as Far future) were selected as representatives for the future simulation. The relative changes of
 208 streamflow in these two future periods compared to the historical period and the contributions of different runoff
 209 components to discharge in these representative time periods were particularly calculated to evaluate the future changes.
 210

211 3. Results

212 3.1 Streamflow change characteristic during the historical period

213 As shown in Table 6, the annual runoff at four stations in the YTR basin did not exhibit a significant trend over the
 214 past six decades. The annual runoff of the three upper stations (Lazi, Nugesha and Yangcun) showed a decreasing trend



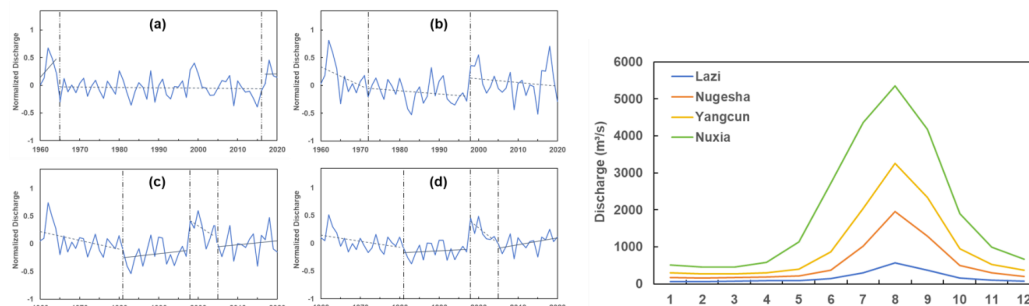
215 while that of outlet station (Nuxia) exhibited an increasing trend, but all these trends were insignificant. Figure 3 presents
 216 the annual runoff process divided by abrupt change years at the four stations. The change-point of annual runoff was
 217 different among four stations, but 1998 was a common turning year when an abrupt runoff change occurred at three of the
 218 stations.

219 Figure 4 shows the average monthly runoff at four stations. The runoff was mostly contributed by summer (June to
 220 August) and autumn (September to November) runoff, accounting for ~50% and ~30% of the annual runoff, respectively
 221 (Table 6). As for the spatial variation, the measured runoff at different stations appeared to be consistent overall, showing
 222 similar intra-annual distribution of monthly runoff, but the changing rates of annual and seasonal runoff were different
 223 among stations. The summer and winter runoff at the four stations all displayed a decreasing and increasing trend,
 224 respectively, while the changes of autumn runoff were all consistent with the annual runoff. The spring runoff at the upper
 225 stations (Lazi and Nugesha) displayed significant changes.

226 **Table 6** Abrupt change points and trend testing results of annual and seasonal streamflow in the historical period (1960–2020) at the four hydrological
 227 stations of the YTR basin.

Station	Abrupt change points of annual streamflow		Variation trends of annual and seasonal streamflow (mm/a) *					Contributions of seasonal streamflow to the annual streamflow (%)			
	Primary	Secondary	Annual	Spring	Summer	Autumn	Winter	Spring	Summer	Autumn	Winter
Lazi	1965	2017	-0.16	+0.23*	-0.58	-0.27	+0.01	12.0	48.8	30.2	9.0
Nugesha	1972	1998	-0.16	-0.16*	-0.37	-0.22	+0.05	9.1	50.7	31.8	8.4
Yangcun	1998	1981, 2005	-0.09	-0.02	-0.05	-0.30	+0.11	8.0	52.0	32.2	7.8
Nuxia	1998	1981, 2005	+0.02	+0.10	-0.20	+0.15	+0.14	9.4	53.1	30.5	7.0

228 a: The annotation “*” indicates a significant change (at the 0.05 level of significance).



229 **Figure 3** (Left) Annual runoff process divided by abrupt change years at the 4 stations of the YTR basin. (a)–(d) for Lazi, Nugesha, Yangcun and Nuxia,
 230 respectively.
 231

232 **Figure 4** (Right) Average monthly runoff during 1960–2020 at the 4 stations of the YTR basin.

234 3.2 Model performance obtained by different calibration variant

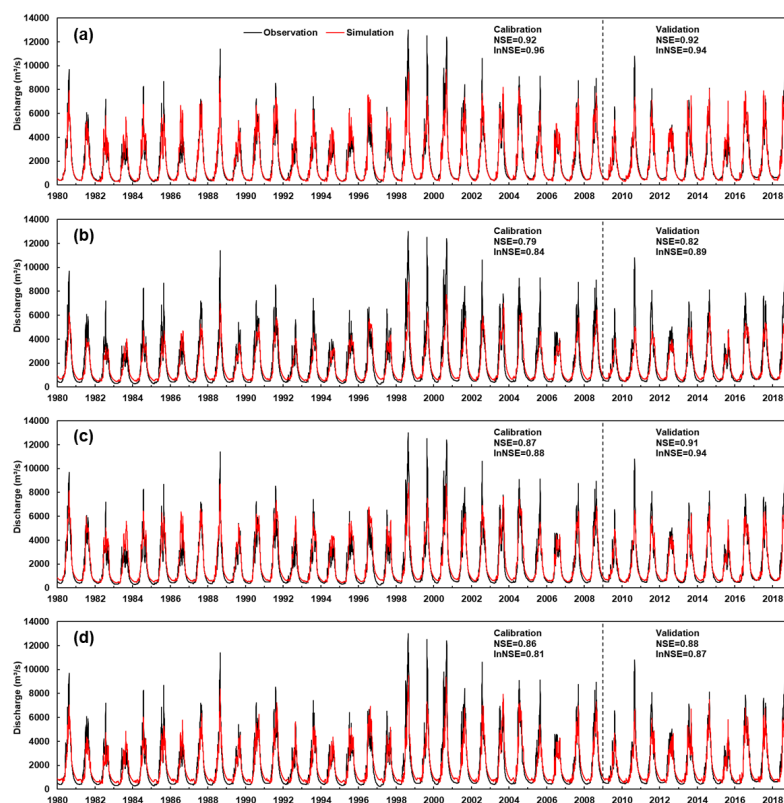
235 Figure 5 shows the observed and simulated discharges at the Nuxia station for calibration and validation periods by
 236 various calibration variants. The THREW model performed well in discharge simulation under these variants and almost
 237 all of their NSE and lnNSE values during the calibration and validation periods were beyond 0.8, with some of them
 238 exceeding 0.9. But with regard to the simulation of other elements, different variants performed variously. The
 239 performances of SWE, SCA and GMB simulations and the specific evaluation metrics are shown in Fig. 6 and Table 7.

240 Seasonal and interannual variations in SWE, SCA and GMB were reproduced well by calibration variant “DSG”,
 241 indicated by the low values of $RMSE_{SWE}$, $RMSE_{SCA}$, and $RMSE_{GMB}$. Due to the uncertainty of the observed Snow Depth



242 product and the relatively simplified calculation process of SWE, the variations of SWE were not simulated as well as
 243 other elements, but the average simulated SWE was close to the average observation, indicating that the amount of
 244 snowpack was reproduced well. In comparison, variant “DG” significantly overestimated the SWE, as indicated by the
 245 high $RMSE_{SWE}$, while an obvious overestimation of GMB simulation occurred in the variant “DS”, with a high value of
 246 $RMSE_{GMB}$. The variant “D” performed the worst overall, along with the most significant overestimation of SWE, obvious
 247 bias of GMB and high values of $RMSE_{SWE}$ and $RMSE_{GMB}$. For the calibration of snow, SWE played a more pronounced
 248 constraint role, while SCA’s constrain was easier to be satisfied. The values of $RMSE_{SCA}$ in these four variants were all
 249 relatively low (~ 0.10), but the simulated SCA processes of variant “DG” and “D” were higher than observation, while the
 250 peaks were a bit underestimated by other two variants (Fig. 6).

251 To summarize, variations of all elements (discharge, SWE, SCA and GMB) were reproduced well by calibration
 252 variant “DSG”, effectively utilizing all observed data. Comparatively, variant “DG” and “DS” performed poorly in the
 253 simulation of snow and glacier process respectively, whereas the single-objective variant “D” presented poor performances
 254 in simulation of all the elements except for the discharge. Thus, among these four different variants, arguably the variant
 255 “DSG” with the most objectives in calibration could achieve the comprehensively best result.



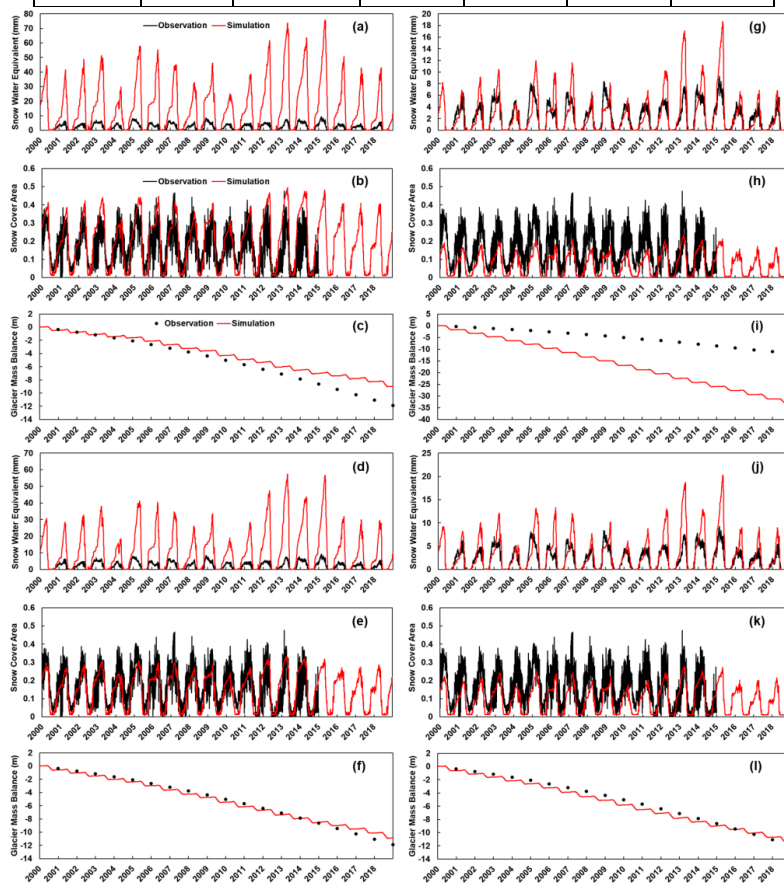
256
 257 **Figure 5** Annual discharge processes of observation and simulation at the Nuxia station during 1980–2018 by various calibration variants. (a)–(d) for
 258 calibration variant “D”, “DG”, “DS”, “DSG”, respectively.

259 **Table 7** Calibrated and validated results at Nuxia station by various calibration variants.

Element	Metrics	Period	Calibration variant			
			D	DG	DS	DSG



Discharge	NSE	1980–2009	0.92	0.79	0.87	0.86
		2010–2018	0.92	0.82	0.91	0.88
		1980–2009	0.92	0.80	0.88	0.87
	lnNSE	1980–2009	0.96	0.84	0.88	0.81
		2010–2018	0.94	0.89	0.94	0.87
		1980–2018	0.95	0.85	0.89	0.82
SWE	RMSE	2000–2009	1.79	1.20	0.19	0.24
		2010–2018	2.30	1.61	0.27	0.33
		2000–2018	2.05	1.41	0.23	0.28
SCA	RMSE	1981–2009	0.07	0.06	0.12	0.10
		2010–2014	0.13	0.08	0.10	0.08
		1981–2014	0.08	0.07	0.11	0.10
GMB	RMSE	2000–2009	0.14	0.10	1.20	0.12
		2010–2018	0.28	0.20	1.07	0.17
		2000–2018	0.22	0.15	1.14	0.14



260

261

Figure 6 Annual processes of SWE, SCA and GMB of observation and simulation in the whole YTR basin (Nuxia station) during 2000–2018 by various

262

calibration variants. (a–c), (d–f), (g–i) and (j–l) for calibration variant “D”, “DG”, “DS”, “DSG”, respectively.

263

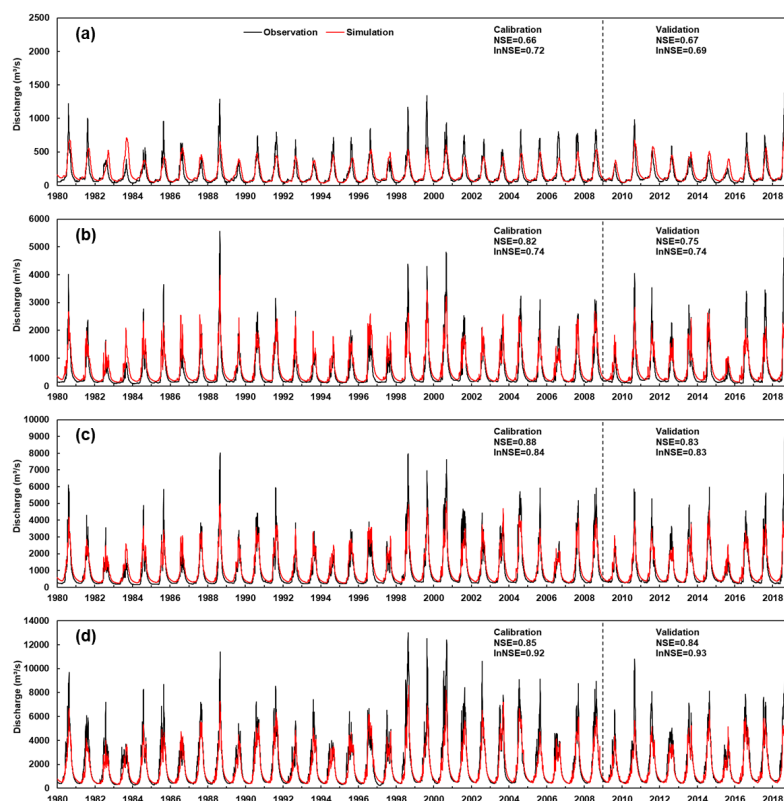


264 Then we further focused on the simulations of upstream stations and the calibration variant “ALL” was set as a
 265 supplement. The simulation results at all hydrological stations in the YTR basin by calibration variant “DSG” and “ALL”
 266 are shown in Table 8. Although the two variants achieved similar performance at the outlet station (Nuxia), both well
 267 reproducing the processes of discharge, SWE, SCA and GMB, there were significant differences in the results at the
 268 upstream stations. The variant “ALL” obviously performed better in the simulation of upstream stations, with high values
 269 of NSE and lnNSE ($NSE > 0.8$ and $\lnNSE > 0.7$ at Yangcun and Nugesha stations, NSE and $\lnNSE > 0.6$ at Lazi station)
 270 and low values of $RMSE_{SWE}$, $RMSE_{SCA}$, and $RMSE_{GMB}$ during the calibration and validation periods, while variant “DSG”
 271 had significant deviations, especially for the most upstream Lazi station. Therefore, variant “ALL” was considered to have
 272 further improvements compared to variant “DSG”, which could better simulate the hydrological processes in different
 273 regions of the basin. Figure 7 and 8 present the observed and simulated discharges and other calibration elements at all
 274 stations of the YTR basin under the variant “ALL”. The simulated discharge process of all stations coincided with the
 275 observed process on the whole, and for the processes of SWE, SCA and GMB in different regions, they were also close to
 276 the observed processes overall.

277
 278
 279

Table 8 Calibrated and validated results at all hydrological stations in the YTR basin by calibration variant “DSG” and “ALL”.

	Calibration/Validation /the entire study period		DSG				ALL			
			Nuxia	Yangcun	Nugesha	Lazi	Nuxia	Yangcun	Nugesha	Lazi
Discharge	NSE	1980–2009	0.86	0.80	0.66	-0.31	0.85	0.88	0.82	0.66
		2010–2018	0.88	0.80	0.72	-0.24	0.84	0.83	0.75	0.67
		1980–2009	0.87	0.80	0.68	-0.29	0.85	0.86	0.80	0.66
	lnNSE	1980–2009	0.81	0.51	0.19	-0.48	0.92	0.84	0.74	0.72
		2010–2018	0.87	0.58	0.31	-0.58	0.93	0.83	0.74	0.69
		1980–2018	0.82	0.52	0.22	-0.50	0.92	0.83	0.74	0.72
SWE	RMSE	2000–2009	0.24	0.29	0.38	0.73	0.21	0.25	0.34	0.68
		2010–2018	0.33	0.42	0.56	1.07	0.29	0.37	0.50	1.02
		2000–2018	0.28	0.36	0.48	0.91	0.25	0.31	0.42	0.86
SCA	RMSE	1981–2009	0.10	0.07	0.06	0.11	0.11	0.08	0.05	0.09
		2010–2014	0.08	0.07	0.08	0.14	0.09	0.07	0.06	0.11
		1981–2014	0.10	0.07	0.06	0.12	0.11	0.07	0.05	0.10
GMB	RMSE	2000–2009	0.12	0.16	0.12	0.07	0.08	0.07	0.08	0.15
		2010–2018	0.17	0.25	0.26	0.21	0.21	0.16	0.17	0.20
		2000–2018	0.14	0.21	0.20	0.15	0.15	0.12	0.13	0.18



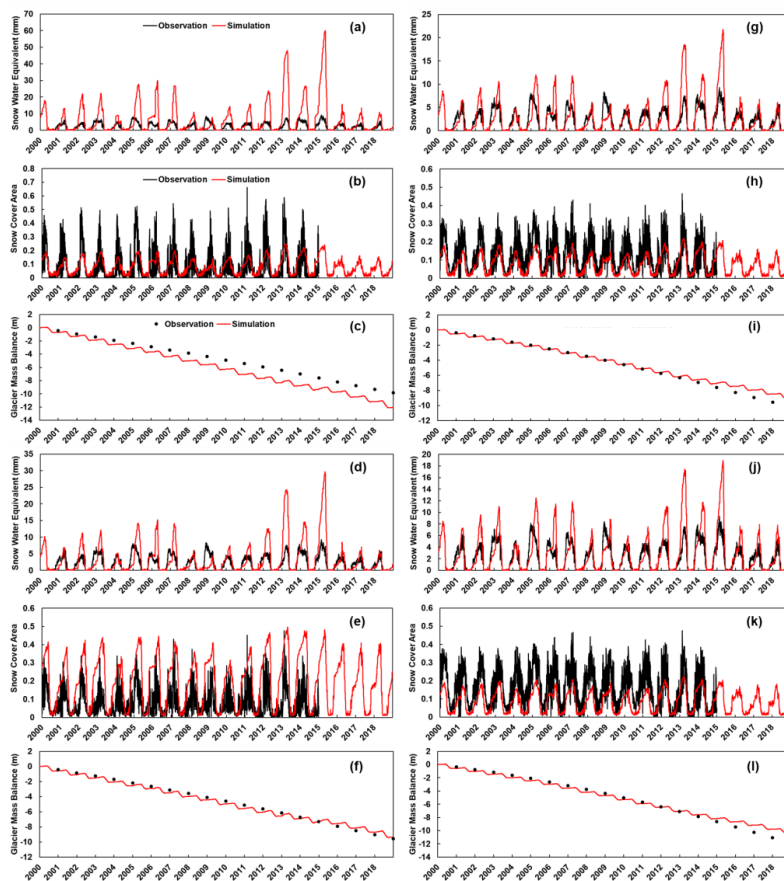
280

281

282

Figure 7 Annual discharge processes of observation and simulation at four stations in the YTR basin during 1980–2018 by calibration variant “ALL”.

(a)–(d) for Lazi, Nugesha, Yangcun, Nuxia station, respectively.



283
284 **Figure 8** Annual processes of SWE, SCA and GMB of observation and simulation in various regions of the YTR basin during 2000–2018 by calibration
285 variant “ALL”. (a–c), (d–f), (g–i) and (j–l) for the region to Lazi, Nugesha, Yangcun, Nuxia station, respectively.
286

287 3.3 Contributions of each runoff component to streamflow

288 Table 9 shows the contributions of different runoff components to streamflow during the simulation period (1980–
289 2018) at Nuxia station estimated by various calibration variants. Although the discharge variation was well reproduced by
290 all variants in the calibration and validation periods, the contributions of runoff components were quite different among
291 different variants. In all calibration variants, rainfall was the dominant water source with contribution higher than 70%.
292 The contribution of glacier melt was estimated lower than 10%, while the contribution of snowmelt varied significantly
293 among different variants. For the calibration variant “DSG”, the mean contributions of rainfall, snowmelt, and glacier melt
294 to annual streamflow in the YTR basin were around 88.8%, 4.9%, and 6.3%, respectively. In variant “DG”, the contribution
295 of glacier melt to streamflow was 6.3%, same as that of the “DSG” variant, but the contribution of snowmelt was much
296 higher (16.7%). Conversely in variant “DS”, the contribution of snowmelt to streamflow was 4.5%, close to that of the
297 variant “DSG”, yet the contribution of glacier melt was higher (9.7%). Regarding the variant “D”, the contributions of
298 runoff component were similar to variant “DG”, but the contribution of snowmelt was even higher, close to 20%.
299 The differences above in contributions of runoff components were basically consistent with the model performance on the
300 simulation of each element. Considering the overall performances, the result of variant “DSG” was regarded as the most



301 reliable one of these four variants, as it minimized the uncertainty of simulation on various elements.
 302 Comparing the variant “DSG” and “ALL”, the contributions of runoff components to streamflow at the Nuxia station
 303 obtained by the two variants were similar, with snowmelt and glacier melt together accounting for 11~12%. However, as
 304 for upstream stations, the contributions of meltwater runoff in the upstream stations under variant “DSG” were quite small
 305 (<10% at Yangcun and Nugesha stations, and <20% at Lazi station), while the result obtained by variant “ALL” was a
 306 bit different. Snowmelt and glacier melt runoff accounted for a larger proportion in upstream stations. The contributions of
 307 snowmelt and glacier melt runoff during 1980–2018 were 7.5%, 5.1% at Yangcun station, 8.9%, 5.3% at Nugesha station,
 308 and 23.9%, 11.6% at Lazi station, respectively. The contributions of snowmelt and glacier melt runoff in different regions
 309 would vary due to factors like the difference in snow and glacier coverage within the region, and the spatial variation of
 310 degree-day factors (Zhang et al., 2006). Owing to the calibration results at upstream stations, the runoff composition results
 311 at different stations under the variant “ALL” were believed to be more reasonable.

312 **Table 9** Contributions of different runoff components to discharge during 1980–2018 at the Nuxia station by various calibration variants and at upper
 313 stations by calibration variant “DSG” and “ALL”.

Component (%)	Calibration variant / station										
	D	DG	DS	DSG				ALL			
	Nuxia			Nuxia	Yangcun	Nugesha	Lazi	Nuxia	Yangcun	Nugesha	Lazi
Rainfall	74.4	77.0	85.8	88.8	90.9	90.3	82.7	87.8	87.4	85.8	64.5
Snowmelt	19.6	16.7	4.5	4.9	5.1	5.8	10.3	6.0	7.5	8.9	23.9
Glacier	6.0	6.3	9.7	6.3	4.0	3.9	7.0	6.2	5.1	5.3	11.6

314

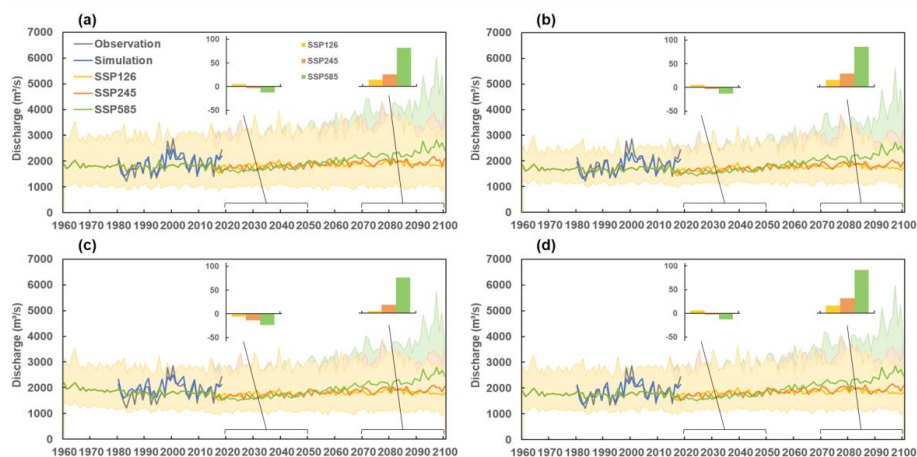
315 3.4 Projection of future streamflow

316 Figure 9 shows the average annual discharge simulated with 10 CMIP6 GCMs during 1960–2100 at the Nuxia station
 317 by the model calibrated by four variants. In spite of the deviations among GCMs and the different parameters obtained by
 318 different calibration variants, the annual mean streamflow in the YTR basin was projected to increase consistently in the
 319 future. The runoff increased insignificantly under SSP126 and SSP245 scenarios, while the increasing trend under SSP585
 320 scenario was visible. Figure 9 also shows the relative changes of annual discharge under three SSP scenarios in the near
 321 and far future period. Here we can find that under some SSP scenarios (mainly SSP245 and SSP585), there could also be
 322 a slight decrease in total runoff in the near future, which was compatible with the results in the previous study (Cui et al.,
 323 2023). But in the far future, the total runoff showed a notable increase under three SSP scenarios by all calibration variants.
 324 For instance, under the calibration variant “DSG”, the relative change of annual streamflow depth at the Nuxia station was
 325 6.0mm (2.2%) / -3.0mm (-1.1%) / -13.1mm (-4.8%) under SSP126/245/585 scenario respectively in the near future period
 326 (2020-2049) compared to the historical period (1960–2009), and was 16.2mm (6.0%) / 31.4mm (11.6%) / 90.9mm (33.6%)
 327 for the same condition in the future period (2070–2099).

328 Table 10 provides the specific average variation trends during different periods simulated with 10 CMIP6 GCMs.
 329 Under different variants, the increasing trend of streamflow under SSP585 scenario at Nuxia Station were all projected to
 330 exceed 1.7mm/a during the future period (2015–2100), especially the far future period (all >2.3mm/a). But under SSP126
 331 scenario, the annual total streamflow showed a downward trend in the far future period and under SSP245 scenario, the
 332 variation trends of streamflow in the far future period were low (most <0.1mm/a). Moreover, the future streamflow of all
 333 the upstream stations also presented an increasing trend (Fig. 10), but their increasing trends were not so significant as the
 334 outlet station (Nuxia). Under the variant “ALL”, the variation trend of streamflow at Nuxia station was about 1.92mm/a
 335 during 2015–2100 under SSP585 scenario, while the trends of streamflow at Yangcun, Nugesha and Lazi station were 1.47,



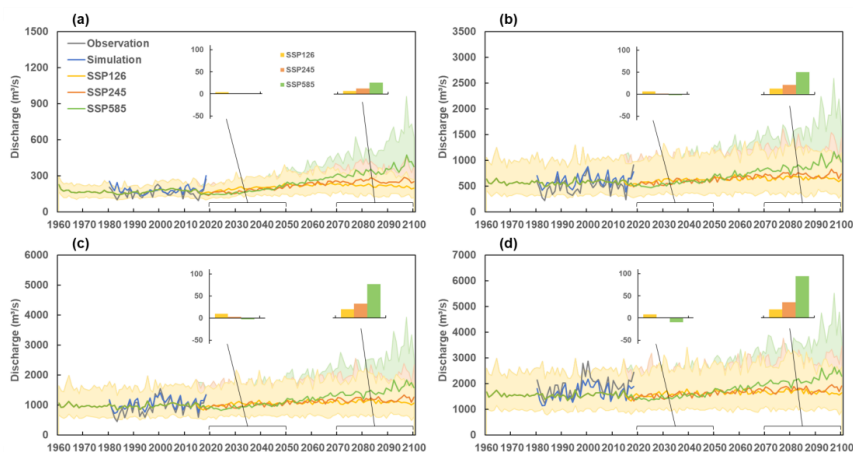
336 0.99 and 0.50mm/a, respectively. Similar to the Nuxia station, the total runoff of the upstream station exhibited relatively
 337 small changes in the near future period, while showed significant changes in the far future period. Compared to the
 338 historical period, the relative change of annual streamflow depth in the far future period was 26.6mm (102.8%), 50.3mm
 339 (57.7%), 76.2mm (51.0%) and 94.6mm (39.9%), respectively at Lazi, Nugesha, Yangcun and Nuxia station under SSP585
 340 scenario.



341 **Figure 9** Average annual discharge simulated with 10 CMIP6 GCMs during 1960–2100 at the Nuxia station by the calibrated model by four variants (the
 342 grey line is the observed value, the blue line is the simulated value in calibration, and the shaded area indicates the deviations of 10 GCMs data). (a)–(d)
 343 for calibration variant “D”, “DG”, “DS”, “DSG”, respectively.
 344

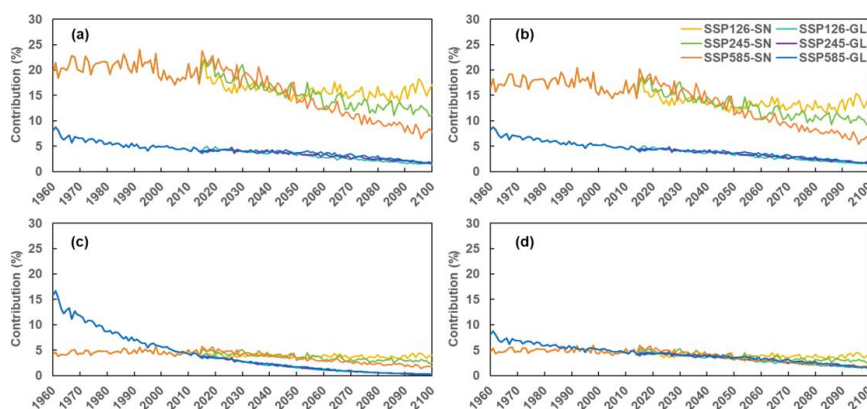
345 **Table 10** Average variation trends during different periods at the Nuxia station by various calibration variants and at upper stations by calibration variant
 346 “ALL” simulated with 10 CMIP6 GCMs.

Variation trend (mm/a)	Calibration variant / station								
	D	DG	DS	DSG	ALL				
	Nuxia				Nuxia	Yangcun	Nugesha	Lazi	
1960–2014	0.01	0.05	-0.69	0.03	0.07	0.12	0.05	0.03	
2015–2100	SSP126	0.25	0.25	0.24	0.27	0.27	0.24	0.18	0.08
	SSP245	0.57	0.62	0.62	0.68	0.69	0.56	0.40	0.23
	SSP585	1.73	1.81	1.82	1.92	1.92	1.47	0.99	0.50
1980–2009 (Historical)	0.47	0.55	0.05	0.52	0.56	0.55	0.30	0.22	
2020–2049 (N-Fu)	SSP126	0.54	0.60	0.40	0.59	0.58	0.49	0.37	0.26
	SSP245	0.45	0.52	0.40	0.57	0.57	0.45	0.34	0.25
	SSP585	1.21	1.25	1.09	1.30	1.25	1.04	0.74	0.38
2070–2099 (F-Fu)	SSP126	-0.21	-0.33	-0.21	-0.28	-0.30	-0.14	-0.07	-0.12
	SSP245	0.03	-0.02	0.15	0.11	0.08	0.05	0.03	0.04
	SSP585	2.40	2.37	2.63	2.60	2.50	1.94	1.34	0.59



347
348 **Figure 10** Average annual discharge simulated with 10 CMIP6 GCMs during 1960–2100 at four stations in the YTR basin by the calibrated model by
349 calibration variant “ALL” (the grey line is the observed value, the blue line is the simulated value in calibration, and the shaded area indicates the
350 deviations of 10 GCMs data). (a)–(d) for Lazi, Nugesha, Yangcun, Nuxia station, respectively.

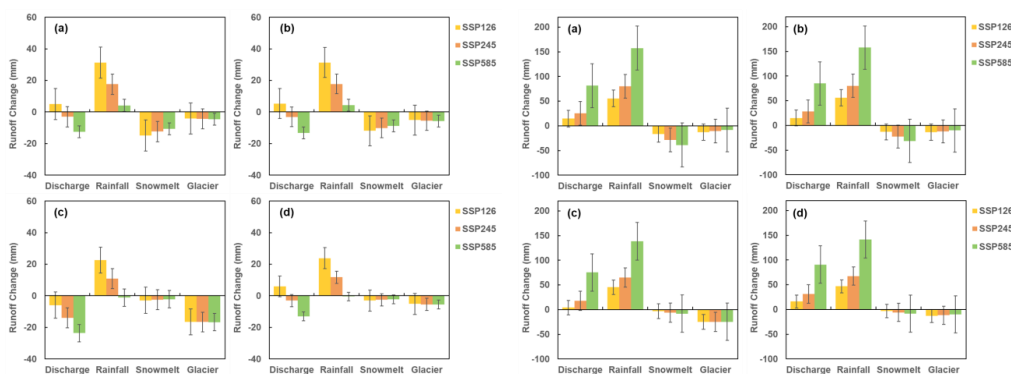
351 Despite the similar future trend of total streamflow, the changes of its components were different among variants, as
352 shown in Fig. 11. With the rising precipitation and temperature, the contributions of both snowmelt and glacier melt would
353 decrease in the future. The decreasing trend of snowmelt/glacier melt runoff was more rapid in the variants estimating
354 higher contributions of the corresponding runoff component. The amounts and contribution proportions of snowmelt and
355 glacier melt runoff exhibited a significant decreasing trend, regardless of the calibration variants and SSP scenarios. The
356 decreasing snowmelt runoff was due to the reduced snowfall caused by climate warming, while the reduced glacier melt
357 runoff indicated that the effect of shrinking glacier areas was more dominant than the acceleration of glacier melting caused
358 by global warming. For instance, in the calibration variant “DSG”, the glacier area in the YTR basin by the end of 2100
359 was only about 37%, 33% and 25% of that in 2010s under three SSP scenarios, respectively.



360
361 **Figure 11** Average annual snowmelt runoff and glacier melt runoff simulated with 10 CMIP6 GCMs during 1960–2100 at the Nuxia station by the
362 calibrated model by four calibration variants (The abbreviation SN and GL represent snowmelt and glacier melt runoff, respectively). (a)–(d) for
363 calibration variant “D”, “DG”, “DS”, “DSG”, respectively.



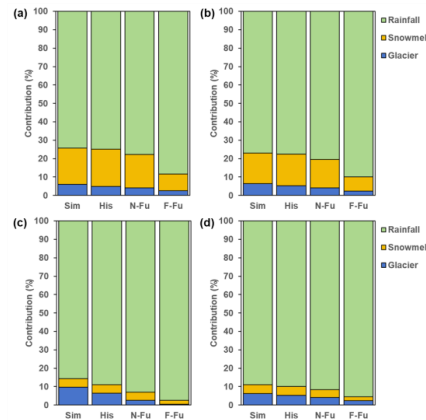
364 More visible results of the changes of various runoff compositions can be seen in Fig. 12 and 13, which shows the
 365 relative changes of annual discharge and different runoff components under three SSP scenarios in the near future (2020–
 366 2049) and far future period (2070–2099), respectively, compared to the historical period (1980–2009) at the Nuxia station
 367 estimated by four calibration variants. The reduction in snowmelt runoff was most notable under SSP585 scenario in the
 368 far future due to the most significant increase in temperature, while the reduction of glacier melt runoff did not differ that
 369 significantly under different SSP scenarios. The contribution of meltwater in variant “DSG” was relatively small, so the
 370 decrease in meltwater runoff due to the rising temperature played a less significant role, and the increase in total runoff in
 371 the future was more significant compared to other calibration variants, which was also reflected by the more significant
 372 variation trends of streamflow in variant “DSG” (Table 10). The most significant decreasing streamflow was estimated by
 373 the “DS” calibration variant that estimated the highest contribution of glacier melt runoff among variants, which seemed
 374 counterintuitive. This is because of the most significant shrinkage of glacier coverage area caused by the fast glacier melting
 375 rate compared to other variants. In specify, the glacier area in the YTR basin by the end of 2049 simulated by the “DS”
 376 variant was only about 40% of that in 2010s under SSP245 scenario, while this proportion was approximately 68% for the
 377 “DSG” variant.



378
 379 **Figure 12** (Left) Relative changes of annual discharge and different runoff components under three SSP scenarios in the Near future period (2020–2049)
 380 compared to the historical period (1980–2009) at the Nuxia station estimated by four calibration variants (error bars represent one standard deviation).
 381 (a)–(d) for calibration variant “D”, “DG”, “DS”, “DSG”, respectively

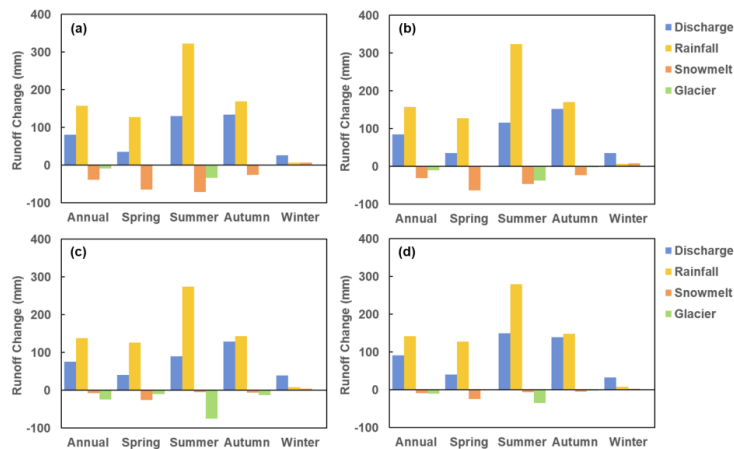
382 **Figure 13** (Right) Relative changes of annual discharge and different runoff components under three SSP scenarios in the Far future period (2070–2099)
 383 compared to the historical period (1980–2009) at the Nuxia station estimated by four calibration variants (error bars represent one standard deviation).
 384 (a)–(d) for calibration variant “D”, “DG”, “DS”, “DSG”, respectively.

385
 386 Figure 14 presents the average contributions of different runoff components to discharge in different periods under
 387 SSP585 scenario at the Nuxia station estimated by four calibration variants. The contributions of runoff components in the
 388 historical period estimated by the model driven by the bias-corrected CMIP6 data was similar to that driven by original
 389 input dataset (CMFD and ERA5), illustrated by the “Sim” and “His” columns. Under the most extreme scenario (i.e.
 390 SSP585), the sum contribution of snowmelt and glacier melt runoff could decrease from 10% to less than 5% in calibration
 391 variant “DSG” and “DS” (Fig. 14 (a) and (c)), and from over 20% to less than 10% in variant “DG” and “D” (Fig. 14 (b)
 392 and (d)), in which the contribution of glacier melt runoff would be only about 1–2% under SSP585 scenario in the far
 393 future. Because of the high contribution of rainfall runoff, the increasing precipitation was the determining factor causing
 394 the rising future runoff in the YTR basin, and the rainfall runoff would play a more dominant role in the total runoff in the
 395 near and far future periods compared to the historical period.



396
 397 **Figure 14** Contributions of different runoff components to discharge in the calibration period (i.e. 1980–2018, represented by “Sim”), and the historical
 398 period (1980–2009), near future period (2020–2049), and far future period (2070–2099) under SSP585 scenario (represented by “His”, “N-Fu” and “F-
 399 Fu”, respectively) at the Nuxia station estimated by four calibration variants. (a)–(d) for calibration variant “D”, “DG”, “DS”, “DSG”, respectively.

400 For intra-annual variations, Fig. 15 shows the relative changes of annual and seasonal discharge and different runoff
 401 components under SSP585 scenario in the far future period compared to the historical period at the Nuxia station estimated
 402 by four calibration variants. With regard to different calibration variants, the similar result was that the reduction of
 403 snowmelt runoff (the orange column) in the far future period was most remarkable in spring and summer, while the decrease
 404 of glacier melt runoff (the green column) was most significant in summer. The Calibration variant “DG” estimated most
 405 significant decreasing snowmelt runoff in spring (−63.1mm, −35.8%), and the variant “D” estimated most significant
 406 decreasing snowmelt runoff in summer (−71.3mm, 78.1%). The annual decrease in summer glacier melt runoff was most
 407 marked in variant “DS” (−75.0mm, −92.0%). Meanwhile, despite the decreasing snowmelt and glacier melt runoff, the
 408 discharge in the YTR basin in the far future period was expected to increase in all the four seasons, mainly owing to the
 409 increasing rainfall. The rainfall runoff was estimated to increase in the future evidently in spring, summer and autumn,
 410 especially in summer (>270mm, ~25% in all variants).

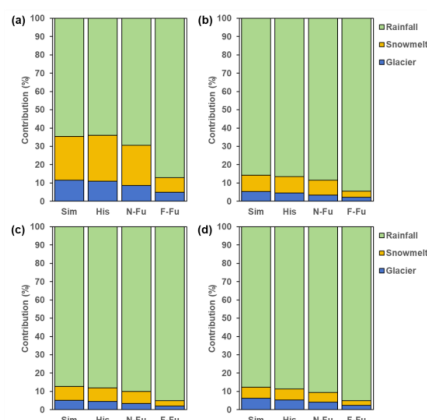


411
 412 **Figure 15** Relative changes of annual and seasonal discharge and different runoff components under SSP585 scenario in the far future period (2070–
 413 2099) compared to the historical period (1980–2009) at the Nuxia station estimated by four calibration variants. (a)–(d) for calibration variant “D”, “DG”,



414 “DS”, “DSG”, respectively.

415 As for spatial diversity, the changes of different runoff components at upstream stations were further examined. Figure
 416 16 shows the average contributions of different runoff components to discharge in different periods under SSP585 scenario
 417 at all stations in the YTR basin estimated by calibration variant “ALL”. Similar to the results above at Nuxia station, the
 418 contributions of snowmelt and glacier melt runoff at upstream stations all displayed a significant decrease trend under
 419 SSP585 scenario in the far future period. Up to the far future, the sum contribution of snowmelt and glacier melt runoff
 420 could decrease from ~35% to ~10% at Lazi station, which possessed the highest contribution of melting runoff in the
 421 historical period, and from over 10% to less than 5% at other stations (Nugesha, Yangcun and Nuxia) under SSP585
 422 scenario. On the whole, the future variations of runoff and its components at upstream stations were consistent with the
 423 outlet station.



424
 425 **Figure 16** Contributions of different runoff components to discharge in the calibration period (i.e. 1980–2018, represented by “Sim”), and the historical
 426 period (1980–2009), near future period (2020–2049), and far future period (2070–2099) under SSP585 scenario (represented by “His”, “N-Fu” and “F-
 427 Fu”, respectively) at four stations in the YTR basin estimated by calibration variant “ALL”. (a)–(d) for Lazi, Nugesha, Yangcun, Nuxia station,
 428 respectively.

430 4. Discussion

431 4.1 Influence of runoff component apportionment on streamflow projection

432 Four different calibration variants for the whole basin were adopted in this study to examine the effects of various
 433 observational datasets on the model simulation, and the contributions of different runoff components and the future
 434 streamflow projected by the model calibrated under each calibration variant were assessed furthermore. Compared to the
 435 variant utilizing all the observational data for calibration, the main differences of other variants could be attributed to two
 436 situations: one is the variant with snow unconstrained and the other is the variant with glacier unconstrained. It was
 437 observed that in the case of unconstrained snow, the contribution of snowmelt runoff to discharge was relatively high, while
 438 in the case of unconstrained glacier, the contribution of glacier melt runoff was relatively high in the historical period,
 439 which might be overestimated apparently compared to the actual situation. Furthermore, adding the observational datasets
 440 of upstream stations for calibration could further improve the distribution of the model and reduce simulation deviations
 441 in different regions within the basin.

442 For the future projection, the streamflow simulated by models under different calibration variants was similar in
 443 general in terms of interannual variation and average seasonal distribution. However, the overestimate of the contribution



444 of snowmelt and glacier melt runoff could lead to underestimation of the increasing trends of future runoff by approximately
445 5~10%. The reduction of snowmelt runoff was more marked in the projection under the variant with snow unconstrained
446 and similar results occurred in the projection under the variant with glacier unconstrained, in which the decrease of glacier
447 melt appeared to be more significant.

448 The calibration variants had an impact on the variation trend of streamflow in the near future period and under low
449 emission scenario (SSP126), while the impact was not significant in the far future period and under high emission scenarios
450 (SSP245 and SSP585). Under all calibration variants, the total streamflow would significantly increase in the far future,
451 along with the overwhelmingly dominated role of rainfall runoff in the streamflow and the substantially reduced meltwater
452 runoff. Furthermore, the significant decrease in snowmelt and glacier melt runoff as well as their contributions to
453 streamflow in the future also occurred to the upstream stations. Altogether, it is beneficial to utilize more observational
454 data to constrain the model in calibration, to obtain better simulation results and understand more accurate contributions of
455 runoff components, so as to obtain more reliable projection of future streamflow's change and changes of various elements.

456 **4.2 Comparison with other studies**

457 Table 11 summarizes the contributions of snowmelt and glacier melt runoff to discharge and future projection results
458 in the YTR basin in previous studies and this study. Various hydrological models with different characteristics were used
459 in the hydrological simulation of the YTR basin, including SRM, SPHY, VIC, CREST etc., and divergences existed in the
460 results of runoff component apportionment and future streamflow projection. For instance, the contribution of snowmelt
461 and glacier melt runoff to the total runoff could both range from less than 10% to over 30%. In some studies, the
462 contribution of snowmelt runoff was significantly higher than that of glacier melt (e.g. Zhang et al., 2013 and Su et al.,
463 2016), while some other studies presented the opposite situation with glacier melt runoff taking a larger contribution than
464 the snowmelt (e.g. Lutz et al., 2014 and Feng, 2020). Nevertheless, the contributions of snowmelt runoff and glacier melt
465 runoff were close in some studies (Chen et al., 2017), and some others did not distinguish between the two components or
466 only considered one of them (e.g., Bookhagen and Burbank, 2010 and Gao et al., 2019). Moreover, some of the previous
467 studies also carried out the future runoff's projection in the YTR basin, most of which used the CMIP5 GCMs, while the
468 results of future streamflow changes, including the changes of snowmelt and glacier melt runoff also differed.

469 In comparison, the contributions of snowmelt and glacier melt runoff to the total runoff in the YTR Basin in our study,
470 constrained by all observational data (discharge, SWE, SCA and GMB), are lower than the results in most previous studies.
471 The divergence of the results could be attributed to several factors. The first and most critical factor is the data used to
472 force and calibrate the model. Constraining the model parameters by the observation datasets related to snow and glacier
473 could brought confidence to the runoff component partitioning. Our results indicated that calibrating the model without
474 snow depth and glacier mass balance datasets resulted in overestimation of meltwater, which was consistent with the fact
475 that the studies not adopting these two datasets estimated much higher contribution of meltwater than our study (e.g., Zhang
476 et al., 2013).

477 The second factor is the definition of runoff component. Although the terms "snowmelt runoff" and "glacier melt
478 runoff" were adopted in all the studies, they actually referred to different things. Our study considered snow and glacier
479 meltwater as input water sources, while the baseflow from groundwater was not considered as a component. This is because
480 the groundwater was fed by the infiltrated water, which could be finally tracked to the three water sources. But some studies
481 regarded the baseflow as a coordinate component with rainfall and meltwater (e.g., Lutz et al., 2014), thus the
482 rainfall/meltwater runoff in those studies may only refer to the surface runoff induced by the corresponding water source.
483 The results also depended on the calculation equation of the reported contribution ratio. For example, Chen et al. (2017)
484 adopted the similar definition as us and utilized SCA, SWE and total water storage datasets to constrain snow and glacier



485 simulation, but the contribution ratio was about twice of our results. This is because they calculated the contribution by
 486 dividing the meltwater by the total streamflow, which was about half of the denominator adopted in our study (the sum of
 487 rainfall, snowmelt and glacier melt) due to evaporation.

488 Furthermore, the simulation of snow and glacier processes also influenced the runoff component. For instance, if the
 489 sublimation during snowfall was not simulated, the contribution of snowmelt runoff may be overestimated. Also, whether
 490 to consider the glacier area and how to simulate its changes could also impacted the results (e.g. Immerzeel et al., 2010,
 491 Lutz et al., 2014, Gao et al., 2019). If the influence of reduction in glacier area exceeds that of the acceleration of glacier
 492 melting caused by rising temperature, the amount of glacier melt runoff would decrease, then affecting the total runoff
 493 variation (e.g. Immerzeel et al., 2010 and this study). On the contrary, the situation that the reduction of glacier area was
 494 offset by the acceleration of glacier melting might lead to different results of the streamflow change (e.g. Lutz et al., 2014).

495 As for the future projection, in addition to the differences discussed above, the factors affecting the model results also
 496 included the differences between CMIP5 and CMIP6 data, whether the GCMs data was corrected and the reference for
 497 correction, as well as the chosen projection period. For example, the precipitation was overestimated for WATCH forcing
 498 data (WFD) in the TP, and using it as for GCMs data's correction would lead to a higher streamflow in the future (e.g. Xu
 499 et al., 2019). And the changes of streamflow had different variations in different time periods, as our study presented.
 500 Generally, the streamflow exhibited an increase trend in the far future, but in the near future, the variation might be different
 501 (e.g. Immerzeel et al., 2010, Su et al., 2016, Zhao et al., 2019).

502 **Table 11** Contributions of snowmelt and glacier melt runoff to discharge and future projection results modelled in the YTR basin in previous studies

Relevant studies /Reference	Hydrological Model	Data for calibration, hydrological station used	Period	Streamflow contribution	Future projection, future streamflow changes ^a	Notes
Bookhagen and Burbank, 2010	SRM, based on satellite-derived snow cover, surface temperature, and solar radiation	Observed discharge; not mentioned the calibration station	2000–2007	Snow and glacier melt (without distinction): 34.3% (May–Oct: 29.1%)	No	Discharge = rain + snow – ET
Immerzeel et al., 2010	SRM	Observed discharge; not mentioned the calibration station	2000–2007	Snow and glacier melt (without distinction): 27%	Yes, use 5 GCMs (A1B scenario, 2046–2065) Streamflow ↓ (19.6%, the best-guess glacier scenario) Rainfall ↑ Glacier ↓	
Zhang et al., 2013	VIC-glacier (VIC combined with a degree-day glacier algorithm)	Observed discharge; Nuxia	1961–1999	Snow: 23.0% Glacier: 11.6%	No	
Lutz et al., 2014	SPHY, with a degree-day snow and glacier melting model	Observed discharge; not mentioned the calibration station	1998–2007	Snow: 9.0% Glacier: 15.9% (Rainfall: 58.9% Baseflow: 16.2%)	Yes, use 4 CMIP5 GCMs (RCP4.5/8.5, 2041–2050) Streamflow ↑ (4.5/5.2%) Snow: 7.8/7.2% (↓) Glacier: 13.7/13.6% (↓) Rainfall: 61.4/61.6% (↑) Baseflow: 17.5/17.6% (↑)	Runoff = rainfall + snow melt + glacier melt + baseflow
Su et al., 2016	VIC-glacier	Observed discharge and precipitation; Nuxia	1971–2000	Snow: ~23% Glacier: ~12%	Yes, use 20 CMIP5 GCMs (RCP2.6/4.5/8.5, 2011–2040, 2041–2070) Streamflow ↑ Rainfall ↑ Snow ↓ Glacier ↑ Contribution of snow and glacier melt: total–, Snow ↓ Glacier ↑	
Chen et al., 2017	CREST (improved)	Observed discharge, SWE, SCA, satellite-derived TWS (total water storage); Nuxia	2003–2014	Snow: 10.6% Glacier: 9.9%	No	Total runoff = rainfall + snow meltwater + glacier meltwater –



						outflow of held water
Gao et al., 2019	HBV	Observed discharge; Nuxia	1971–2000	Snowmelt-induced runoff: 24.1~31.4%	Yes, use 18 CMIP5 GCMs (RCP2.6/8.5, 2041–2070, baseline period: 1971–2000) Snowmelt-induced runoff ↓ (8.6/13.1%)	Total runoff = Rainfall – induced runoff + Snowmelt – induced runoff
Zhao et al., 2019	VIC-CAS (coupled with glacier melting and glacier response schemes)	Observed discharge, Glacier distribution; Nuxia	1971–2010	Snow: 23.1% Glacier: 5.5%	Yes, use 5 CMIP5 GCMs (RCP2.6/8.5, 2011–2100) Streamflow ↑ Rainfall ↑ Snow ↓ Glacier ↓	
Xu et al., 2019	THREW	Observed discharge; Nuxia, Bahadurabad	1980–2001	Snow: 20.3% Glacier: 5.3%	Yes, use 5 RCMs (RCP4.5/8.5, 2020–2035) Streamflow ↓ (4.1%) / ↑ (19.9%) Snow: 24.6/20.3% Glacier: 6.1/5.0% Rainfall: 69.3/74.8%	WATCH forcing data for bias-correction Runoff = rainfall + Snowmelt + glacier – Evaporation
Tian et al., 2020	THREW	Observed discharge, SWE; Nuxia	2001–2015	Snow: 20.0% Glacier: 14.0%	No	
Wang et al., 2021	VIC-glacier	Observed discharge, PET; Nuxia	1984–2015	Snow: 15% Glacier: 14%	No	Considering the process of wind blowing snow
Cui et al., 2023	THREW (modified)	Observed discharge, SCA, GMB, Glacier coverage; Nuxia	1985–2014	Snow: 12.7% Glacier: 4.4%	Yes, use 22 CMIP6 GCMs (warming levels of 1.5/2.0/3.0°C) Streamflow ↑ Rainfall ↑ Snow ↓ Glacier ↓ / ↑ Contribution: Rainfall ↑ Snow ↓ Glacier–	
Guo, 2021 (Master's thesis)	SWAT	Observed discharge, SWE, SCA; Lazi, Nugesha, Yangcun, Nuxia	2001–2014	Snow:21.96/6.53/1.91 /4.11% and all ↑ (for the four sub-regions divided by stations)	No	Taking the snow sublimation into account
Xuan, 2019 (Doctoral thesis)	SWAT	Observed discharge; Nugesha, Yangcun, Nuxia	1979–2008	Snow: 20/20/38% Rainfall: 44/47/32% Groundwater: 36/33/30% (for Nugesha 1974 / Yangcun 1961 / Nuxia 1961)	Yes, use 5 GCMs (RCP2.6/8.5) Rainfall ↑ Snow ↑ / ↑ / ↓ Groundwater ↓	Runoff = groundwater + rainfall – induced-runoff + snowmelt – induced runoff
Wang, 2019 (Doctoral thesis)	GBEHM	Observed discharge, Thickness of frozen ground; Nuxia	1981–2010	Glacier: ~5% and ↑	Yes, use 5 CMIP5 GCMs (RCP4.5, 2011–2060) Streamflow ↑ Rainfall ↑ Evaporation ↑	Focus on frozen ground degradation
Feng, 2020 (Doctoral thesis)	SPHY	Observed discharge; Nuxia	1980–2014	Snow: 7.8% Glacier: 30.8% (Rainfall: 52.4% Baseflow: 9.3%)	No	Runoff = rainfall + snow melt + glacier melt + baseflow
This study	THREW	Observed discharge, SWE, SCA, GMB; Lazi, Nugesha, Yangcun, Nuxia	1980–2018	Snow: 23.9/8.9/7.5/6.0%, Glacier: 11.6/5.3/5.1/6.2% (for the drainage areas of 4 stations) (under the “ALL” calibration variant)	Yes, use 10 CMIP6 GCMs(SSP126/245/585, 2020–2049/2070–2099) Streamflow ↓ / ↑ Rainfall ↑ Snow ↓ Glacier ↓ Contribution: Rainfall ↑ Snow ↓ Glacier ↓	Runoff = rainfall + Snowmelt + glacier – Evaporation

503 a: The notations “↑” / “↓” / “–” represent showing a trend of increasing / decreasing / generally unchanged.

504 **4.3 Limitations and perspectives**

505 This study constructed the distributed hydrological model THREW in the YTR basin, and set various calibration
 506 variants to compare the constraint effects of different datasets on the model and analyze the streamflow components and
 507 future runoff changes estimated under different variants. However, there are still some limitations in the current research,



508 which can be further improved in subsequent studies. For instance, the current model reproduced the snow and glacier
509 melting processes well, and newly considered the sublimation of snowfall, with abundant datasets (observed discharge,
510 SWE, SCA, and GMB) to calibrate it. But the calculation of snow sublimation as well as the conversion of snow depth
511 data to SWE were referred to previous study, and the calculation might be a bit rough. Meanwhile, more processes and
512 corresponding data could be incorporated into the hydrological processes, such as the contribution of frozen soil.

513 Secondly, our discussion in this study mostly focused on the annual discharge at the outlet station of the YTR basin.
514 Although some seasonal characteristics and results at upstream stations were also mentioned, the analysis of them was
515 relatively limited. On a more detailed time and spatial scale, there would be more complex variations in runoff changes
516 and its components. So, the subsequent studies could further analyze the runoff changes and its components in different
517 regions within the basin, as well as their characteristics on a smaller time scale. Moreover, the current study mainly focused
518 on the runoff changes and did not consider more socio-economic factors. Yet if combining more factors for analysis, like
519 the population distribution and water demand situation, more practical conclusions may be obtained.

520 **5. Conclusion**

521 Comprehensive observational discharge data at hydrological stations was tested to investigate the historical runoff
522 variations in the YTR basin, and a distributed hydrological model THREW was constructed in the basin to further analyze
523 the runoff components and estimate future runoff changes. In the calibration of the model, different variants were set up to
524 compare the constraint effects of each dataset and their impacts on the results. The main findings are as follows:

- 525 1. In historical periods, there was no significant changes in annual runoff in the YTR basin over the past six decades,
526 with a decrease in upstream stations and an increase in the outlet station. The THREW model constrained by
527 streamflow, snow and glacier datasets indicated that the contributions of snowmelt and glacier melt runoff to
528 streamflow were relatively low for the whole basin, both accounting for about 5–6%. Concretely, the contributions of
529 snowmelt/glacier melt runoff to streamflow were 23.9/11.6%, 8.9/5.3%, 7.5/5.1%, and 6.0/6.2% for Lazi, Nugesha,
530 Yangcun and Nuxia station, respectively.
- 531 2. In the future periods, the annual runoff in the YTR basin exhibited an increase trend, not significantly under the low
532 emission scenarios (SSP126 and SSP245) while significantly under the high emission scenario (SSP585), which
533 occurred at all stations. The relative change of annual streamflow depth in the far future period (2070–2099) compared
534 to the historical period (1980–2009) was 26.6mm (102.8%), 50.3mm (57.7%), 76.2mm (51.0%) and 94.6mm (39.9%)
535 at Lazi, Nugesha, Yangcun and Nuxia station, respectively under the high emission scenario. Furthermore, the amounts
536 and contributions of snowmelt and glacier melt runoff would decrease markedly, with their combined contribution
537 reaching less than 10% at Lazi station and less than 5% at other stations in the far future under the high emission
538 scenario, while the rainfall runoff would play an overwhelmingly dominant role in the total runoff.
- 539 3. Comparing the results of different calibration variants, it was suggested that using more data to calibrate the model
540 played a vital role in reducing the uncertainty of hydrological simulation. The simulation of SWE, SCA, and GMB all
541 could exhibit a significant bias due to the lack of corresponding observational data to constrain the modeling, resulting
542 in the overestimated contributions of snowmelt and glacier melt runoff to streamflow, for nearly 17% and 10%,
543 respectively at the outlet station. Moreover, the overestimation on the contribution of meltwater runoff led to an
544 underestimation of the increasing trends of annual runoff by approximately 5–10% in future projection, along with a
545 faster reduction of the meltwater runoff.



546 **Acknowledgments.**

547 This study has been supported by the National Natural Science Foundation of China (grant nos. 52309023 and
548 51825902) and the Shuimu Tsinghua Scholar Program.

549 **Code and data availability**

550 The CMIP6 model outputs are available at <https://esgf-node.llnl.gov/search/cmip6/>. The ERA5-Land data is
551 available at <https://cds.climate.copernicus.eu/cdsapp#!/dataset/reanalysis-era5-land?tab=overview> (Muñoz Sabater,
552 2019). Other datasets for this study are publicly available as follows: CMFD
553 (<https://doi.org/10.11888/AtmosphericPhysics.tpe.249369.file>, Yang et al., 2019), glacier inventory
554 (<https://doi.org/10.3972/glacier.001.2013.db>, Liu, 2012), glacier elevation change (<https://doi.org/10.6096/13>, Hugonnet
555 et al., 2021), snow depth (<https://doi.org/10.11888/Snow.tpdc.271743>, Yan et al, 2021), snow cover
556 (<https://doi.org/10.1016/j.rse.2018.06.021>, Chen et al., 2018), LAI (<https://lpdaac.usgs.gov/products/mod15a2hv006/>,
557 Myneni et al., 2015), NDVI (<https://doi.org/10.5067/MODIS/MOD13A3.006>, Didan, 2015), and soil property
558 (<https://doi.org/10.1029/2019ms001784>, Dai et al., 2019). The simulated streamflow, snow water equivalent, snow cover,
559 and glacier mass balance data produced by the model will be available at the Zenodo website at the time of publication.

560 **Author contributions.** MJZ and YN conceived the idea and collected the data. MJZ, YN and FT conducted the analysis
561 and wrote the paper.

562 **Competing interests.** At least one of the (co-)authors is a member of the editorial board of Hydrology and Earth System
563 Sciences.

564 **References**

- 565 Bookhagen, B. and Burbank, D. W.: Toward a complete Himalayan hydrological budget: Spatiotemporal distribution of snowmelt and rainfall and their
566 impact on river discharge, *Journal of Geophysical Research–Earth Surface*, 115, <https://doi.org/10.1029/2009jrf001426>, 2010.
- 567 Cannon, A. J.: Multivariate quantile mapping bias correction: an N-dimensional probability density function transform for climate model simulations of
568 multiple variables, *Climate Dynamics*, 50, 31–49, <https://doi.org/10.1007/s00382-017-3580-6>, 2018.
- 569 Chen, X., Long, D., Hong, Y., Zeng, C., and Yan, D.: Improved modeling of snow and glacier melting by a progressive two-stage calibration strategy
570 with GRACE and multisource data: How snow and glacier meltwater contributes to the runoff of the Upper Brahmaputra River basin?, *Water
571 Resources Research*, 53, 2431–2466, <https://doi.org/10.1002/2016wr019656>, 2017.
- 572 Chen, X., Long, D., Liang, S., He, L., Zeng, C., Hao, X., and Hong, Y.: Developing a composite daily snow cover extent record over the Tibetan
573 Plateau from 1981 to 2016 using multisource data, *Remote Sensing of Environment*, 215, 284–299, <https://doi.org/10.1016/j.rse.2018.06.021>, 2018.
- 574 Cui, T., Li, C., and Tian, F.: Evaluation of Temperature and Precipitation Simulations in CMIP6 Models Over the Tibetan Plateau, *Earth and Space
575 Science*, 8, <https://doi.org/10.1029/2020ea001620>, 2021.
- 576 Cui, T., Li, Y., Yang, L., Nan, Y., Li, K., Tudaji, M., Hu, H., Long, D., Shahid, M., Mubeen, A., He, Z., Yong, B., Lu, H., Li, C., Ni, G., Hu, C., and
577 Tian, F.: Non-monotonic changes in Asian Water Towers' streamflow at increasing warming levels, *Nature Communications*, 14,
578 <https://doi.org/10.1038/s41467-023-36804-6>, 2023.
- 579 Dai, Y., Xin, Q., Wei, N., Zhang, Y., Wei, S., Yuan, H., Zhang, S., Liu, S., and Lu, X.: A Global High-Resolution Data Set of Soil Hydraulic and
580 Thermal Properties for Land Surface Modeling, *Journal of Advances in Modeling Earth Systems*, 11, 2996–3023,
581 <https://doi.org/10.1029/2019ms001784>, 2019.



- 582 David, E., David, B., and Christine, A. S.: pySOT and POAP: An event-driven asynchronous framework for surrogate optimization, arXiv preprint
583 arXiv, 1908.00420., <https://doi.org/10.48550/arXiv.1908.00420>, 2019.
- 584 Didan, K.: MOD13A3 MODIS/Terra vegetation Indices Monthly L3 Global 1 km SIN Grid V006, NASA EOSDIS Land Processes DAAC [data set],
585 <https://doi.org/10.5067/MODIS/MOD13A3.006>, 2015.
- 586 Feng, Y.: A Dissertation Submitted to China University of Geosciences for Doctoral Degree, <https://doi.org/10.27493/d.cnki.gzdzy.2020.000100>, 2020.
- 587 Guo R.: Study on snow cover variations and snowmelt runoff modeling in the Yarlung Tsangpo-Brahmaputra River Basin,
588 <https://doi.org/10.1016/j.scitotenv.2019.02.013>, 2021.
- 589 Gao, C., Liu, L., Ma, D., He, K., and Xu, Y.-P.: Assessing responses of hydrological processes to climate change over the southeastern Tibetan Plateau
590 based on resampling of future climate scenarios, *Science of the Total Environment*, 664, 737-752,
591 <https://doi.org/10.27456/d.cnki.gyndu.2021.002615>, 2019.
- 592 Han, P., Long, D., Han, Z., Du, M., Dai, L., and Hao, X.: Improved understanding of snowmelt runoff from the headwaters of China's Yangtze River
593 using remotely sensed snow products and hydrological modeling, *Remote Sensing of Environment*, 224, 44-59,
594 <https://doi.org/10.1016/j.rse.2019.111587>, 2019.
- 595 He, Q., Yang, J., Chen, H., Wang, Y., Tang, F., Ji, Q., and Ge, Q.: Study on hydrological regulation function of glaciers in the cold region basins of
596 western China, *Journal of Glaciology and Geocryology*, 43, 1512-1522, <https://doi.org/10.7522/j.issn.1000-0240.2021.0102>, 2021.
- 597 Hugonnet, R., McNabb, R., Berthier, E., Menounos, B., Nuth, C., Girod, L., Farinotti, D., Huss, M., Dussailant, I., Brun, F., and Kaab, A.: Accelerated
598 global glacier mass loss in the early twenty-first century, *Nature*, 592, 726-731, <https://doi.org/10.1038/s41586-021-03436-z>, 2021.
- 599 Immerzeel, W. W., van Beek, L. P. H., and Bierkens, M. F. P.: Climate Change Will Affect the Asian Water Towers, *Science*, 328, 1382-1385,
600 <https://doi.org/10.1126/science.1183188>, 2010.
- 601 Jiang, Y., Xu, Z., and Xiong, L.: Runoff variation and response to precipitation on multi-spatial and temporal scales in the southern Tibetan Plateau,
602 *Journal of Hydrology-Regional Studies*, 42, <https://doi.org/10.1016/j.ejrh.2022.101157>, 2022.
- 603 Li, D., Lu, X., Overeem, I., Walling, D. E., Syvitski, J., Kettner, A. J., Bookhagen, B., Zhou, Y., and Zhang, T.: Exceptional increases in fluvial
604 sediment fluxes in a warmer and wetter High Mountain Asia, *Science*, 374, 599-603, <https://doi.org/10.1016/j.ejrh.2014.08.004>, 2021.
- 605 Lutz, A. F., Immerzeel, W. W., Shrestha, A. B., and Bierkens, M. F. P.: Consistent increase in High Asia's runoff due to increasing glacier melt and
606 precipitation, *Nature Climate Change*, 4, 587-592, <https://doi.org/10.1126/science.abi9649>, 2014.
- 607 Lan, C., Zhang, Y., Zhu, F., and Liang, L.: Characteristics and changes of streamflow on the Tibetan Plateau: A review, *Journal of Hydrology: Regional
608 Studies*, 2, 49-68, <https://doi.org/10.3972/glacier.001.2013.db>, 2014.
- 609 Liu, S.: The second glacier inventory dataset of China (version 1.0) (2006–2011), National Tibetan Plateau Data Center [data set],
610 <https://doi.org/10.1038/nclimate2237>, 2012.
- 611 Muñoz Sabater, J. (2019): ERA5-Land hourly data from 1950 to present. Copernicus Climate Change Service (C3S) Climate Data Store (CDS). DOI:
612 10.24381/cds.e2161bac (Accessed on 01-Jul-2022)
- 613 Myneni, R., Knyazikhin, Y., and Park, T.: MOD15A2H MODIS/Terra Leaf Area Index/FPAR 8-Day L4 Global 500 m SIN Grid V006, NASA EOSDIS
614 Land Processes DAAC [data set], <https://lpdaac.usgs.gov/products/mod15a2hv006/>, 2015.
- 615 Nan, Y., He, Z., Tian, F., Wei, Z., and Tian, L.: Assessing the influence of water sampling strategy on the performance of tracer-aided hydrological
616 modeling in a mountainous basin on the Tibetan Plateau, *Hydrology and Earth System Sciences*, 26, 4147-4167, <https://doi.org/10.5194/hess-26-4147-2022>, 2022.
- 617 Pettitt, A. N.: A non-parametric approach to the change-point problem, *Applied Statistics*, 28, 126-135, <https://doi.org/10.2307/2346729>, 1979.
- 618 Reggiani, P., Hassanizadeh, S. M., Sivapalan, M., and Gray, W. G.: A unifying framework for watershed thermodynamics: constitutive relationships,
619 *Advances in Water Resources*, 23, 15-39, [https://doi.org/10.1016/s0309-1708\(99\)00005-6](https://doi.org/10.1016/s0309-1708(99)00005-6), 1999.
- 620 Su, F., Zhang, L., Ou, T., Chen, D., Yao, T., Tong, K., and Qi, Y.: Hydrological response to future climate changes for the major upstream river basins in
621 the Tibetan Plateau, *Global and Planetary Change*, 136, 82-95, <https://doi.org/10.1016/j.gloplacha.2015.10.012>, 2016.
- 622



- 623 Tian, F., Hu, H., Lei, Z., and Sivapalan, M.: Extension of the Representative Elementary Watershed approach for cold regions via explicit treatment of
624 energy related processes, *Hydrology and Earth System Sciences*, 10, 619-644, <https://doi.org/10.5194/hess-10-619-2006>, 2006.
- 625 Tian, F., Li, K., Han, S., Nan, Y., and Yang, L.: Dipole spatiotemporal variations of river runoff in Eastern Tibetan Plateau, *Advances in Water Science*,
626 34, 481-489, <https://doi.org/10.14042/j.cnki.32.1309.2020.03.002>, 2023.
- 627 Tian, F., Xu, R., Nan, Y., Li, K., and He, Z.: Quantification of runoff components in the Yarlung Tsangpo River using a distributed hydrological model,
628 *Advances in Water Science*, 31, 324-336, <https://doi.org/10.14042/j.cnki.32.1309.2023.04.001>, 2020.
- 629 Wang, Y.: Simulation and analysis of changes in frozen ground and hydrology in typical basins of the Tibetan Plateau,
630 <https://doi.org/10.27266/d.cnki.gqhau.2019.000058>, 2019.
- 631 Wang, Y., Xie, X., Shi, J., and Zhu, B.: Ensemble runoff modeling driven by multi-source precipitation products over the Tibetan Plateau, *Chinese
632 Science Bulletin-Chinese*, 66, 4169-4186, <https://doi.org/10.1360/tb-2020-1557>, 2021.
- 633 Wang, Y., Wang, L., Zhou, J., Chai, C., Hu, Z., Zhao, L., Wang, S., and Fan, M.: Impacts of frozen ground degradation and vegetation greening on
634 upper Brahmaputra runoff during 1981-2019, *International Journal of Climatology*, 43, 3768-3781, <https://doi.org/10.1002/joc.8057>, 2023.
- 635 Xuan, W.: Impact of climate change on runoff and components based on semi-distributed hydrological model,
636 <https://doi.org/10.1016/j.gloplacha.2019.01.012>, 2019.
- 637 Yan, D., Ma, N., and Zhang, Y.: A daily, 0.05° Snow depth dataset for Tibetan Plateau (2000-2018), *National Tibetan Plateau / Third Pole Environment
638 Data Center [data set]*, <https://doi.org/10.27461/d.cnki.gzjdx.2019.002158>, 2021.
- 639 Yang, K., He, J., Tang, W., Lu, H., Qin, J., Chen, Y., and Li, X.: China meteorological forcing dataset (1979-2018), *National Tibetan Plateau / Third
640 Pole Environment Data Center [data set]*, <https://doi.org/10.11888/Snow.tpcd.271743>, 2019.
- 641 Xu, R., Hu, H., Tian, F., Li, C., and Khan, M. Y. A.: Projected climate change impacts on future streamflow of the Yarlung Tsangpo-Brahmaputra River,
642 *Global and Planetary Change*, 175, 144-159, <https://doi.org/10.11888/AtmosphericPhysics.tpe.249369.file>, 2019.
- 643 Yao, T., Bolch, T., Chen, D., Gao, J., Immerzeel, W., Piao, S., Su, F., Thompson, L., Wada, Y., Wang, L., Wang, T., Wu, G., Xu, B., Yang, W., Zhang, G.,
644 and Zhao, P.: The imbalance of the Asian water tower, *Nature Reviews Earth & Environment*, 3, 618-632, <https://doi.org/10.1038/s43017-022-00299-4>, 2022.
- 645
- 646 Zhang, M., Nan, Y., Wu, Y., Ding, Y., Xu, M. and Tian, F.: Streamflow and sediment change of major rivers in the Eastern Tibetan Plateau from 1960 to
647 2020, *Advances in Water Science*, <https://doi.org/10.14042/j.cnki.32.1309.2024.02.011>, 2024.
- 648 Zhang, Y., Liu, S., and Ding, Y.: Observed degree-day factors and their spatial variation on glaciers in western China, *Annals of Glaciology*, 43, 301-
649 306, <https://doi.org/10.3189/172756406781811952>, 2006.
- 650 Zhang, L., Su, F., Yang, D., Hao, Z., and Tong, K.: Discharge regime and simulation for the upstream of major rivers over Tibetan Plateau, *Journal of
651 Geophysical Research-Atmospheres*, 118, 8500-8518, <https://doi.org/10.1002/jgrd.50665>, 2013.
- 652 Zhao, Q., Ding, Y., Wang, J., Gao, H., Zhang, S., Zhao, C., Xu, J., Han, H., and Shangguan, D.: Projecting climate change impacts on hydrological
653 processes on the Tibetan Plateau with model calibration against the glacier inventory data and observed streamflow, *Journal of Hydrology*, 573, 60-
654 81, <https://doi.org/10.1016/j.jhydrol.2019.03.043>, 2019.
- 655 Zhou, T., Gao, J., Zhao, Y., Zhang, L., and Zhang, W.: Water Vapor Transport Processes on Asian Water Tower, *Bulletin of the Chinese Academy of
656 Sciences*, 34, 1210-1219, <https://doi.org/10.16418/j.issn.1000-3045.2019.11.004>, 2019.
- 657